PNAS
www.pnas.org

Supporting Information for

The functionally relevant site for paxilline inhibition of BK channels

Yu Zhou, Xiao-Ming Xia, Christopher J. Lingle

Corresponding authors: zhouy@wustl.edu; clingle@morpheus.wustl.edu;

This PDF file includes:

Supplementary text
Tables S1-S3
Figures S1-S15
SI References

Supplementary text:

Materials and Methods

Electrophysiology: Details of recording methods for similar experiments have been described recently (1). In brief, all currents were recorded in the inside-out patch configuration with an Axopatch 200B amplifier (Molecular Devices, Sunnyvale, CA) with no leak subtraction. Data were acquired with the Clampex program from the pClamp software package (Molecular Devices, San Jose, CA). During seal formation, an oocyte was bathed in standard frog Ringer (in mM): 115 NaCl, 2.5 KCl, 1.8 $CaCl_2$, 10 HEPES, at pH 7.4. Following patch excision, the pipette tip was moved into flowing test solutions of defined Ca^{2+} concentrations. The pipette/extracellular solution was (in mM): 140 K-methanesulfonate, 20 KOH, 10 HEPES, 2 $MgCl_2$, at pH 7.0. Solutions for application to the cytosolic side of the membrane included (in mM): 140 K-methanesulfonate, 20 KOH, 10 HEPES at pH 7.0. 5 mM HEDTA was used for 10 μM Ca^{2+} and 5 mM EGTA for 0 μM Ca^{2+} solutions. Experiments were performed at room temperature (~22-25 ^{o}C). All chemicals were purchased from Sigma-Aldrich (St. Louis, MO).

Data Analysis. The G-V relationship of BK channels was determined from tail currents measured 150 μs after repolarization to −120 mV. G-V curves were fit by a Boltzmann function

$$G(V) = \frac{G_{\max}}{1 + \exp(-z(V - V_h)/kT)}$$

in which G_{max} is maximal conductance, z is apparent voltage-dependence in units of elementary charge, V_h is the voltage of half-maximal activation, and k and T have their usual physical meanings. The PAX inhibition dose-response relationships were fit by the Hill equation

$$R = \frac{1}{1 + (C / IC_{50})^n}$$

in which R is fractional unblock, C is PAX concentration, IC_{50} is half inhibition concentration, and n is Hill coefficient. Data were analyzed using OriginPro 7.5 (OriginLab Corporation) or programs developed in this laboratory. Error bars in

the figures represent SEMs. Each data point is averaged from at least 4 measurements. Curve fitting results are reported as the fitted values with standard error, which was estimated by OriginPro according to the Error Propagation formula.

SUPPLEMENTARY TABLES

Table S1. The binding energies (kcal/mol) of tremorgenic fungal alkaloids in the closed mSlo1 pore. Only unique poses in the nine most favored binding poses are listed. For tetramerically symmetrical proteins such as the BK channel, each unique pose likely represents one of four identical symmetric positions, although in most evaluations we limited the number of potential poses returned by Autodock to 9.

Paxilline	-8.8	-8.3	-8.2	-7.9
Aflatrem	-10.2	-9.7	-9.4	-9.3
Paspalicine	-9.8	-9.7	-9.7	
Paspalinine	-9.6	-9.2	-9.0	-8.9
Paspalitrem A	-10.2	-10.1	-10.0	
Paspalitrem C	-11.1	-10.1	-10.0	-9.7
Penitrem A	-9.8	-9.5	-9.4	
Verruculogen	-8.2	-7.9	-7.8	

Table S2. The binding energies (kcal/mol) of tremorgenic fungal alkaloids in the open mSlo1 pore. Only unique poses in the nine most favored binding poses are listed.

Paxilline	-8.8	-8.3	-8.3	-8.2
Aflatrem	-9.5	-9.0	-8.9	-8.8
Paspalicine	-9.5	-9.5	-9.5	-9.4
Paspalinine	-9.5	-9.4	-9.3	-9.3
Paspalitrem A	-10.0	-9.9	-9.9	-9.4
Paspalitrem C	-9.6	-9.5	-9.1	-9.0
Penitrem A	-9.5	-9.4	-9.3	-9.1
Verruculogen	-8.5	-8.2	-7.6	-7.6

Table S3. Autodock Vina configuration file used for docking PAX in mSlo1 pore.

```
receptor = mSlo1TM_5tji_6L20_tetra.pdbqt
ligand = Paxilline_HF321.pdbqt
out = mSlo1TM_5tji_6L20_Paxilline_EC.pdbqt
log = mSlo1TM_5tji_6L20_Paxilline_EC_log.txt
```

```
center_x = 172.8
center_y = 172.8
center_z = 143.166
size_x = 45
size_y = 45
size_z = 50

exhaustiveness = 16
```

SUPPLEMENTARY FIGURES

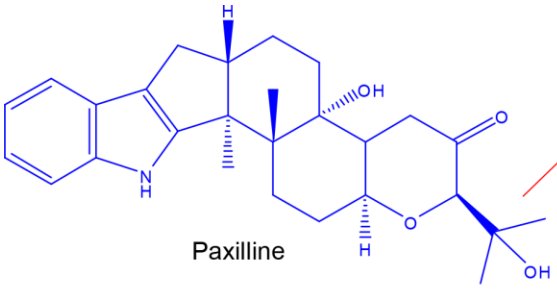

Paxilline

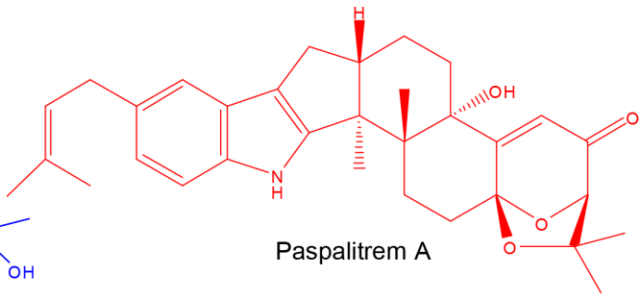

Paspalitrem A

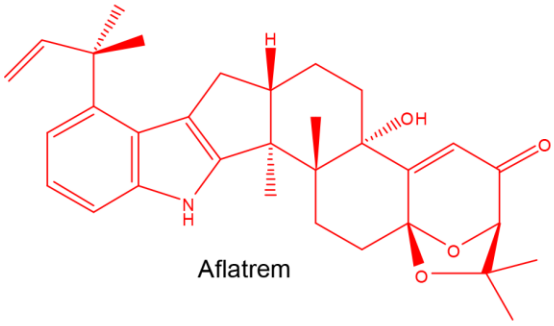

Aflatrem

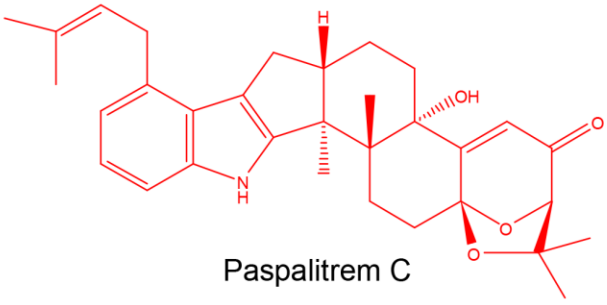

Paspalitrem C

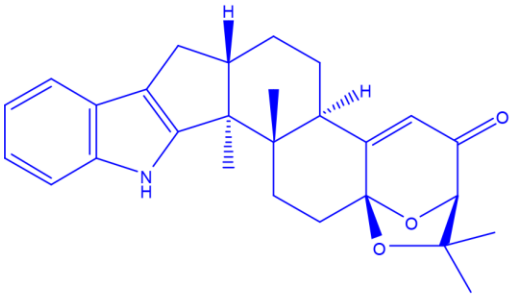

Paspalicine

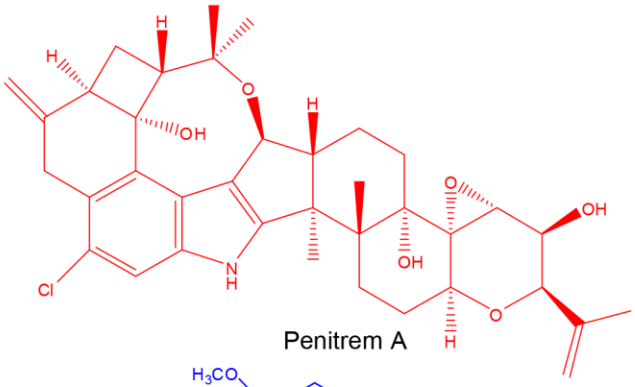

Penitrem A

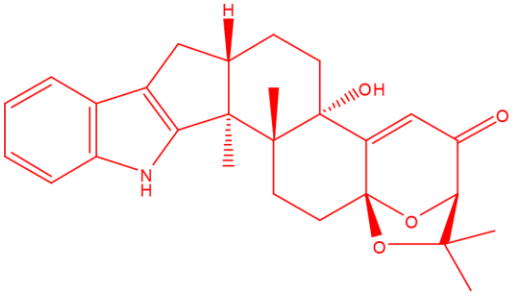

Paspalinine

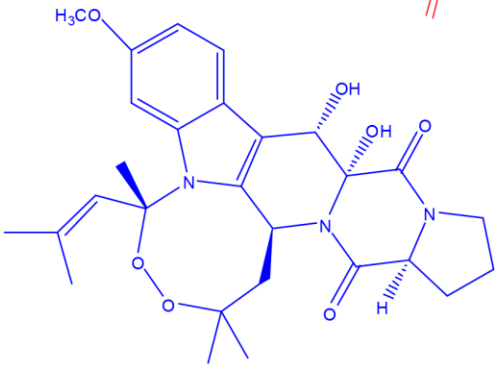

Verruculogen

Fig. S1 Structural formulas of fungal alkaloids that inhibit BK channels and regulate CTX binding. The alkaloids enhancing CTX binding (CTX enhancer) are colored in blue and those reducing CTX binding (CTX reducer) are colored red

Fig. S2 Alignment of aSlo1 and mSlo1 sequences used for homology modeling. The transmembrane segments of aSlo1 are indicated by bars above the sequence alignment (2). The selectivity filter residues are colored in blue. The mSlo1 glycine hinge (G311) is colored in red.

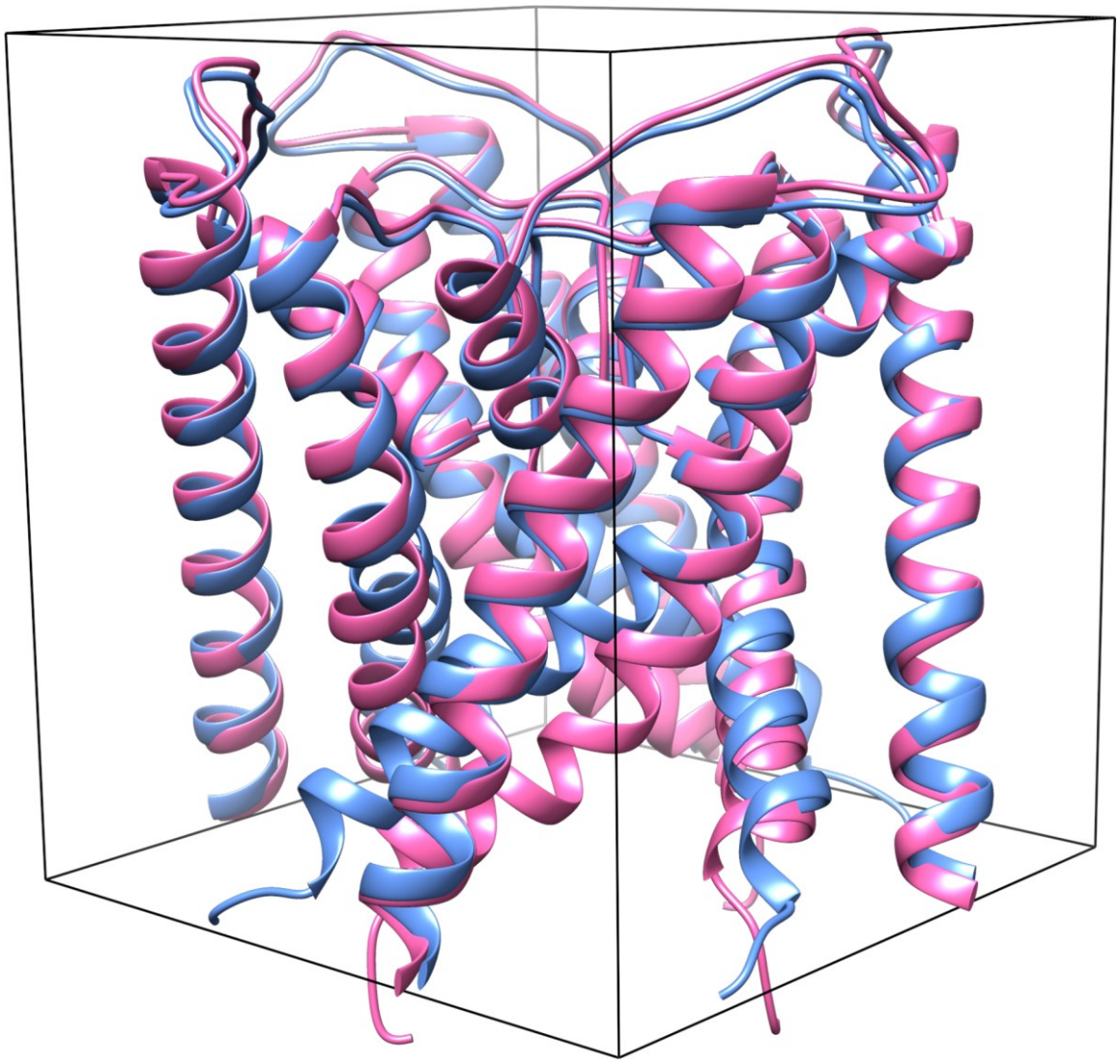

Fig. S3 The default search space for PAX docking in the mSlo1 PGD models. The openand closed mSlo1 models are colored in blue and pink, respectively. The search box with dimension of 45×45×50Å is depicted by black lines.

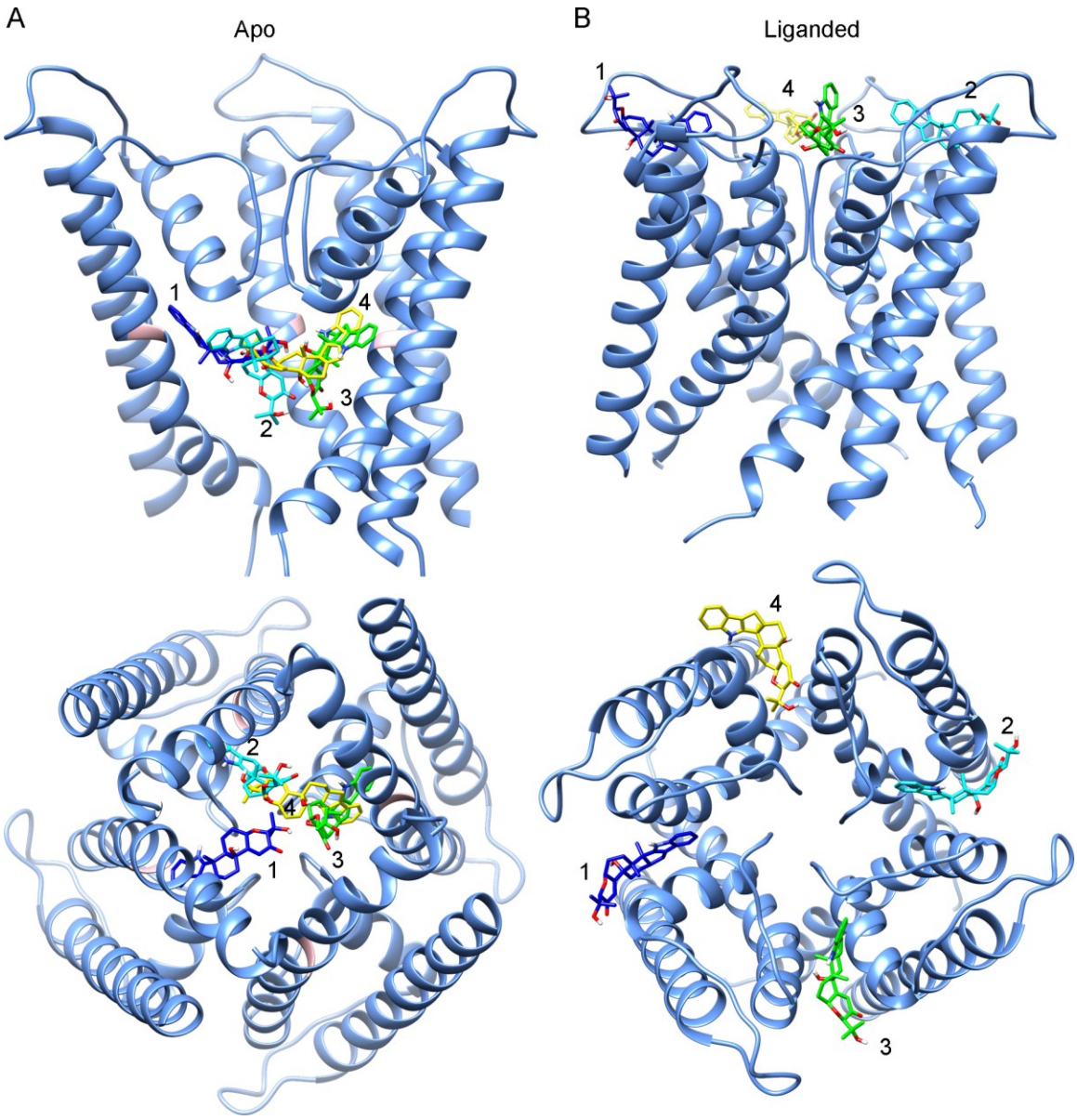

Fig. S4 The four most favored unique PAX binding poses in closed and open mSlo1 models . (A) Side view (top panel) and bottom view (bottom panel) of 4 unique PAX binding poses in the closed mSlo1 pore. The front subunit is removed in the side view for clarity. The binding energies of these poses are (kcal/mol): No. 1 (blue): -8.8, No. 2 (cyan): -8.3, No. 3 (green): -8.2, No. 4 (yellow): -7.9. Compared with the most favored binding pose (No.1), the other binding poses are not only energetically inferior, but also inconsistent with the functional result that PAX inhibition occurs with a Hill coefficient of 1, as these binding poses do not extend into the central cavity to interfere with binding in other identical sites. (B) Side view (top panel) and top view (bottom panel) of the 4 most favored unique PAX binding poses in the open mSlo1 pore. The binding energies of these poses are (kcal/mol): No. 1 (blue): -8.8, No. 2 (cyan): -8.3, No. 3(green): -8.3, No. 4(yellow): -8.2.

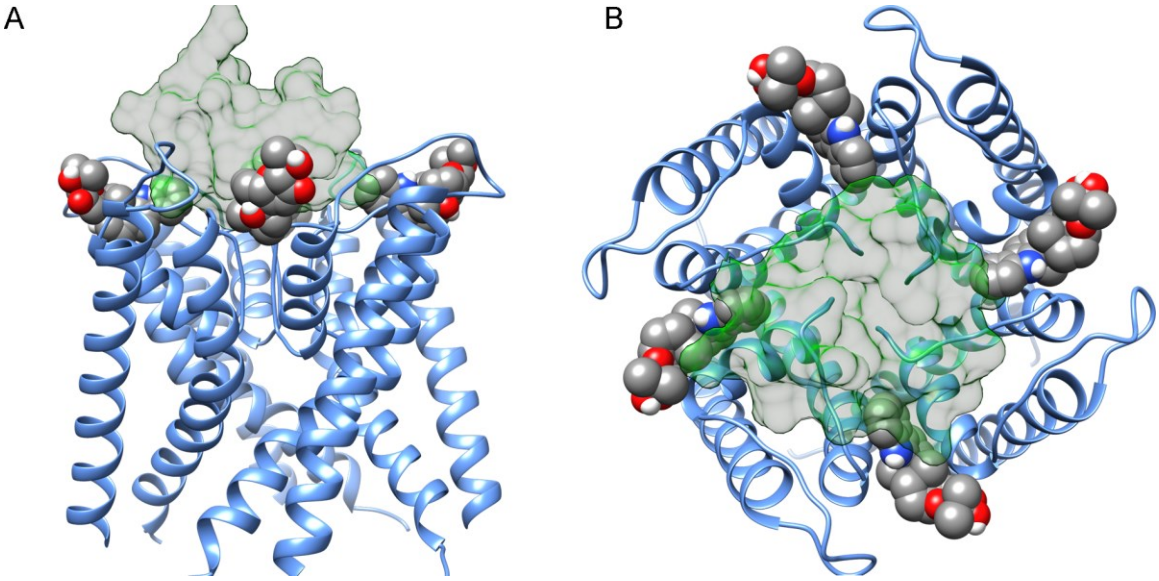

Fig. S5 CTX binding to the extracellular face of the BK channel is likely to be affected by presence of PAX binding. The structure of a chimerical Kv channel/CTX complex (PDB: 4JTD) was aligned with the open mSlo1 structure by their selectivity filters to obtain a theoretical position of CTX occupancy in mSo1. It should be noted that the exact CTX position on the extracellular side of BK channel may not be identical to that of Kv channels, because of differences in the channel turrets and specific side chains (3). However, panel illustrates that positioning of CTX at the extracellular face of a BK channel should partially overlap with at least one of the extracellular PAX binding sites given the size of this toxin and the fact that CTX needs to cover the extracellular entrance of the BK selectivity filter to block the BK channel. Therefore, when PAX molecules occupy all four extracellular binding sites, at least one of them will interfere with CTX binding on the BK channel. For clarity, only CTX (green surface) is shown for the Kv/CTX complex. PAX is rendered as spheres. Panel A is the side view and panel B is a view from the extracellular entrance of BK channel.

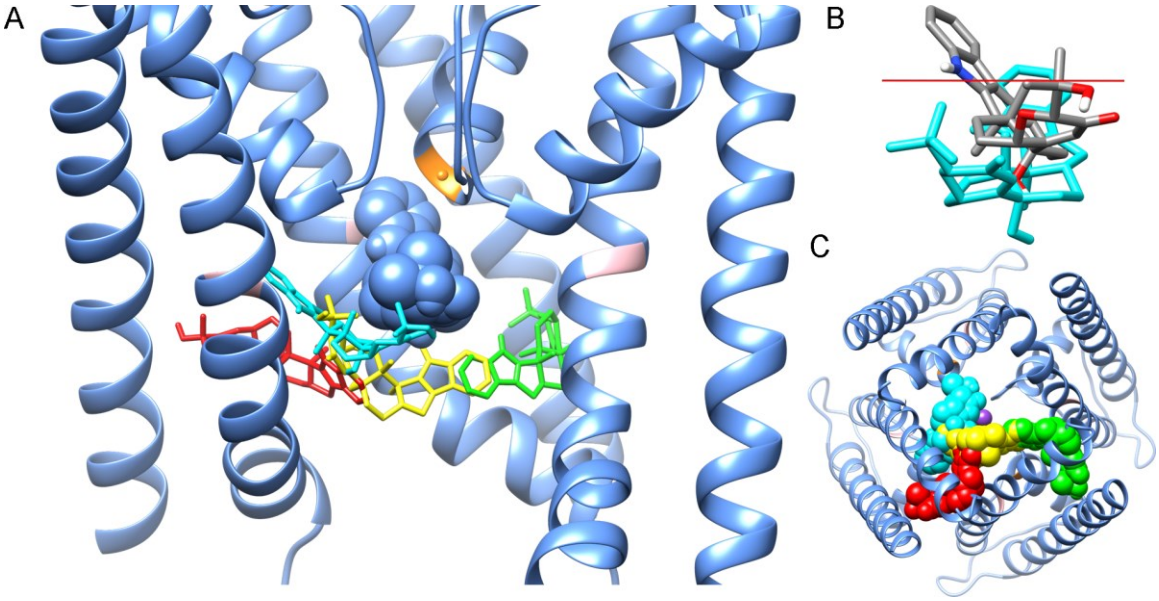

Fig. S6 Binding of one PAX molecule in the S6-Pore helix binding crevice prevents other PAX molecules from adopting the optimal binding pose. (A) The side view of top four unique PAX binding poses in a closed BK pore pre-occupied by a PAX molecule (blue spheres). The front BK subunit is omitted for clarity. G311 is colored in pink. The M285 in the pre-occupied binding crevice is colored in orange. With a PAX molecule predocked in one of the four S6-Pore Helix crevices, the other three identical crevices cannot not be occupied. However, the presence of PAX in one crevice creates *de novo* formation of additional high affinity binding sites, presumably because of additional hydrophobic substrate within the central cavity. For these additional positions, the binding energies (in kcal/mol) estimated by Autodock Vina are: pose No. 1 (cyan): -9.5, pose No. 2 (green): -9.2, pose No. 3 (yellow): -9.1, pose No. 4 (red): -9.0. (B) Binding pose No. 1 (cyan) is compared to the normal PAX binding pose in closed BK pore (colored according to atom, with carbon, oxygen, nitrogen and hydrogen colored in gray, red, blue, and white, respectively.). The red line marks the level of G311 α-carbons to show that the indole ring of binding pose No. 1 is largely outside the binding crevice. (C) The bottom view of top four PAX binding poses (spheres with the same color scheme of panel A) in the PAX/closed BK complex. The PAX molecule predocked in the closed BK pore is omitted to reveal potassium occupancy (purple sphere, from open aSlo1 structure, PDB: 5TJ6) in the BK selectivity filter.

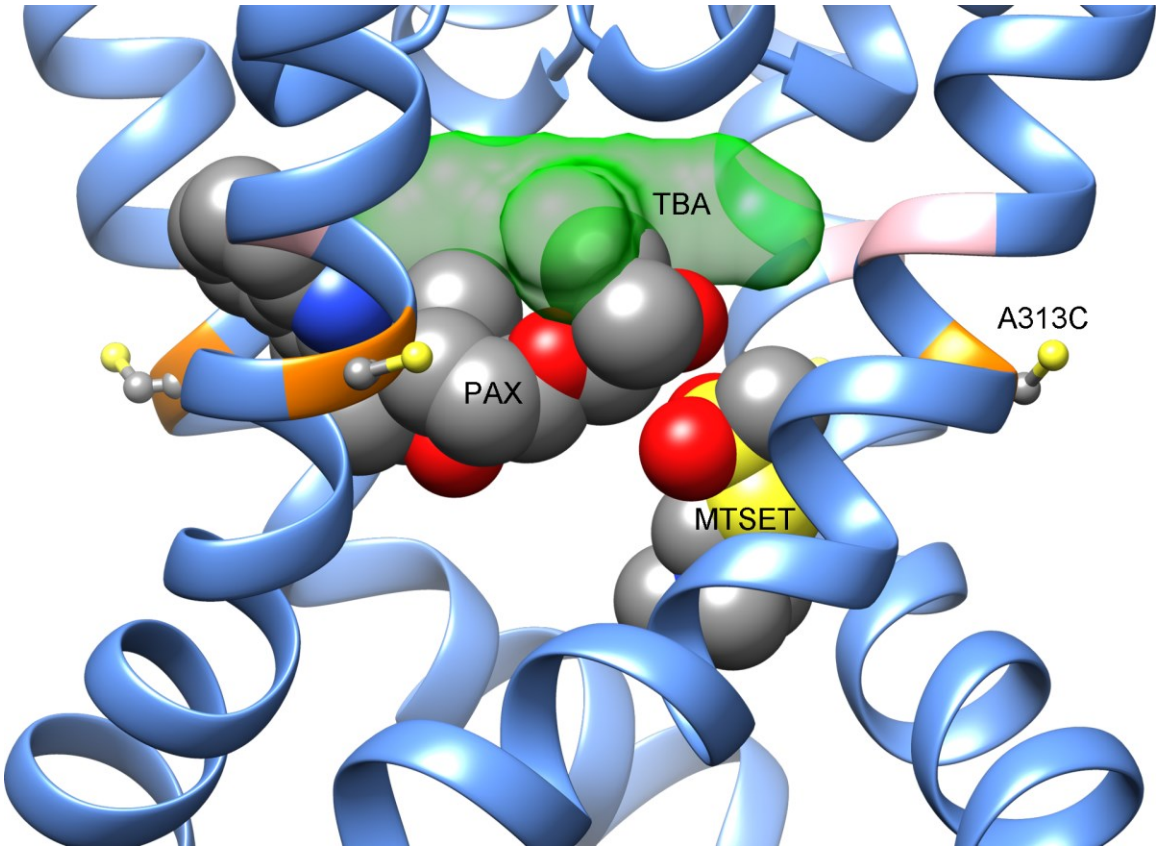

Fig. S7 Binding of PAX in the closed BK pore would be hindered by pore occupancy by QA blockers, but PAX binding would not prevent MTS modification of A313C. The structure of Fab-KcsA-TBA complex (PDB: 2BOB) was aligned with the closed mSlo1 model by their selectivity filters. The mSlo1 pore is rendered as a blue ribbon with G311 colored in pink. For clarity, the front subunit and all S5 segments of mSlo1 are omitted. In addition, TBA, based on its position in the Fab-KcsA-TBA complex, is shown with a green surface. PAX and MTSET are rendered as spheres. MTSET was placed manually inside the BK pore to show that PAX cannot protect all four cysteines at position 313 (ball-and-chain) from being modified by MTSET because of the spacious inner pore of BK channel. It should be noted that the sidechain of A313C does not point into the central ion permeation pathway in this model, while our previous result suggested that A313 is a pore-lining residue as A313C in open BK channels can be modified by MTSET at very high rate (4). There are two possible explanations for such an apparent discrepancy. First, previous studies suggest that BK S6 rotates during activation (5, 6). Thus, the side chain of A313C may rotate away from the central ion permeation pathway in a closed BK channel. Second, the current mSlo1 models are based on the cryo-EM structures of aSlo1 channel, which has two rather bulky residues (isoleucine and phenylalanine) at the glycine hinge position instead of the double-glycine motif found in mammalian BK channels. Thus, the orientations of pore-lining residues and/or gating-associated S6 motion may not be identical between these two types of BK channels.

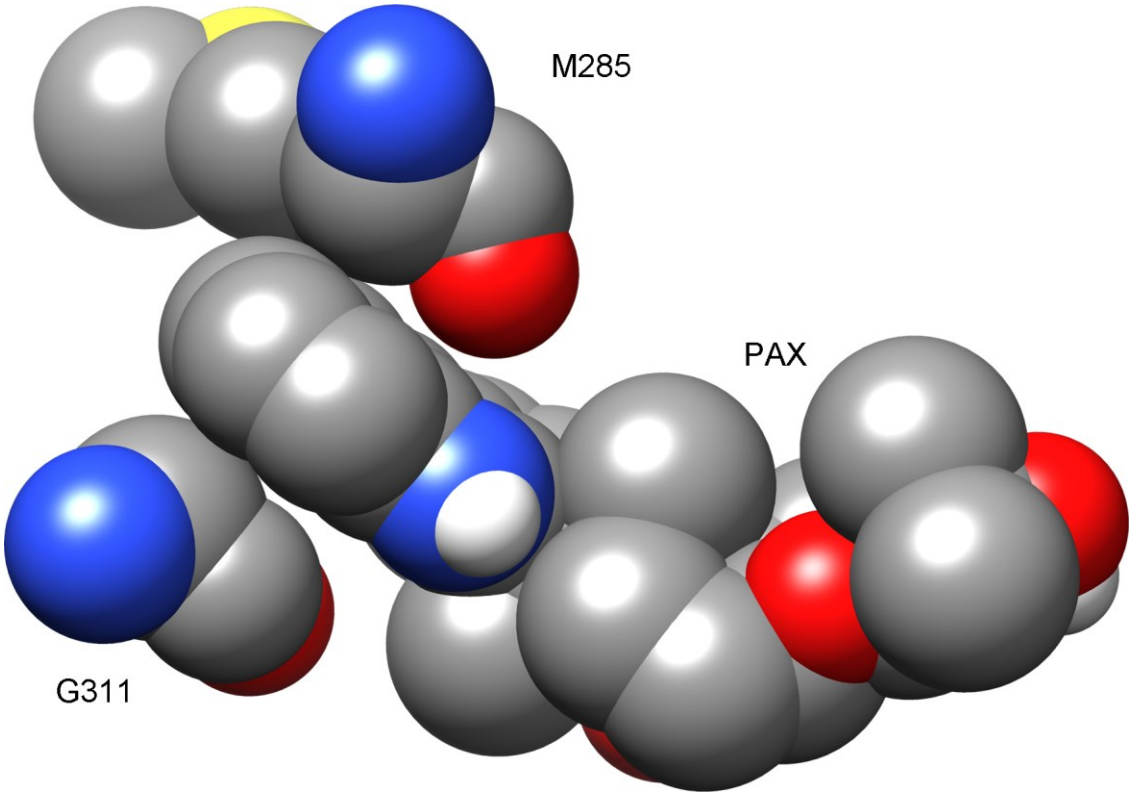

Fig. S8 The side view of PAX in the binding crevice of the closed BK pore. (A) M285, G311 and PAX are all rendered as spheres to show that PAX fits tightly in the S6-Pore helix binding crevice of the closed BK pore without clashing into G311 or M285.

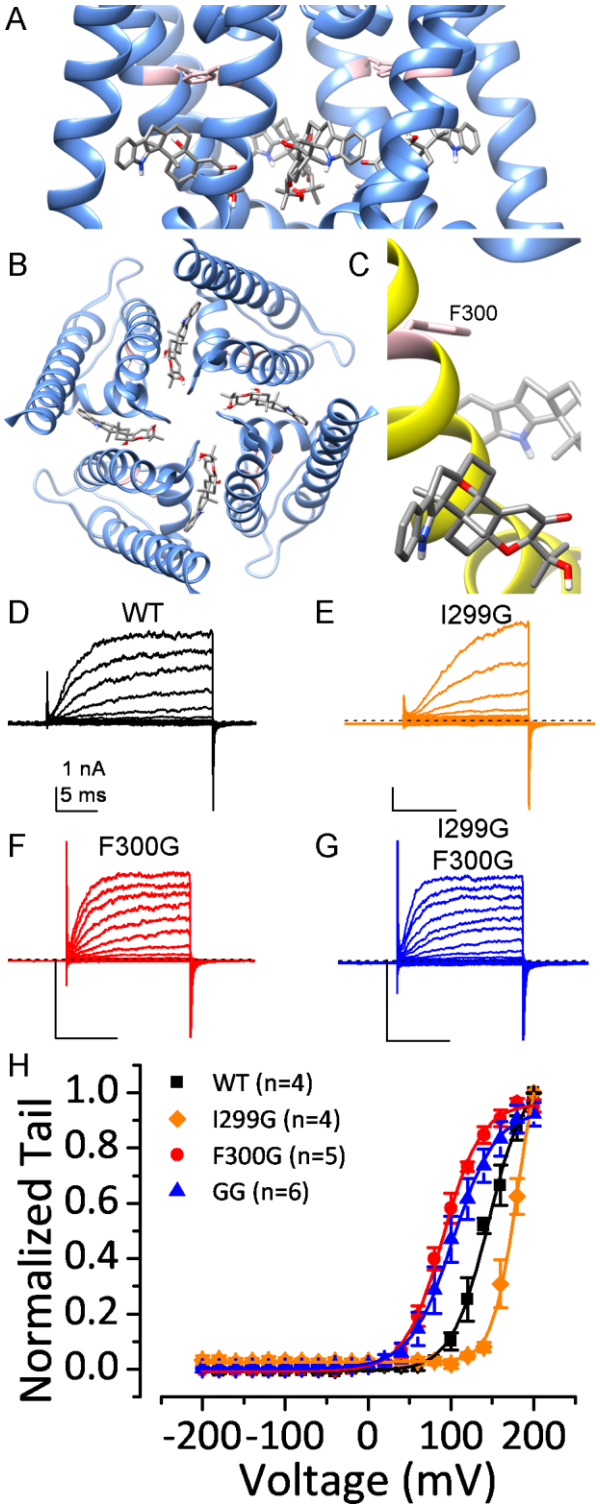

Fig. S9 The most favored binding poses of PAX in the closed aSlo1 pore show that PAX does not occupy the S6-PH crevice in the aSlo1 pore (A) A side view. aSlo1 F300, which is homologous to mSlo1 G311, is colored in pink. (B) A view from the intracellular entrance (C). A close-up view from the same perspective as that in Fig 2. (D-G) Macroscopic currents of WT,

I299G, F300G, and I299GF300G (GG) aSlo1 channels recorded from inside-out patches with 10 μM $[Ca^{2+}]_{in}$. The currents were evoked by steps from -200 to +200 mV with 20-mV increments. The dotted line marks the 0-current level. (H) The G-V relationships of WT (black square), I200G (orange diamond), F300G (red circle) and GG (blue triangle) aSlo1 channels determined from the tail-current of recordings as those shown in panels D-G. The number of experiments contributing to each G-V relationship is listed in parentheses. Boltzmann fit results (solid lines) are: G_{max} = 1.1±0.03, V_h = 145.3±1.6 mV, z = 1.1±0.05e (WT), G_{max} = 1.2±0.07, V_h = 180.5±2.2 mV, z = 1.6±0.11e (I299G), G_{max} = 1.0±0.04, V_h = 90.4±1.0 mV, z = 1.1±0.04e (F300G), G_{max} = 0.9±0.01, V_h = 102.6±1.3 mV, z = 1.0±0.04e (GG).

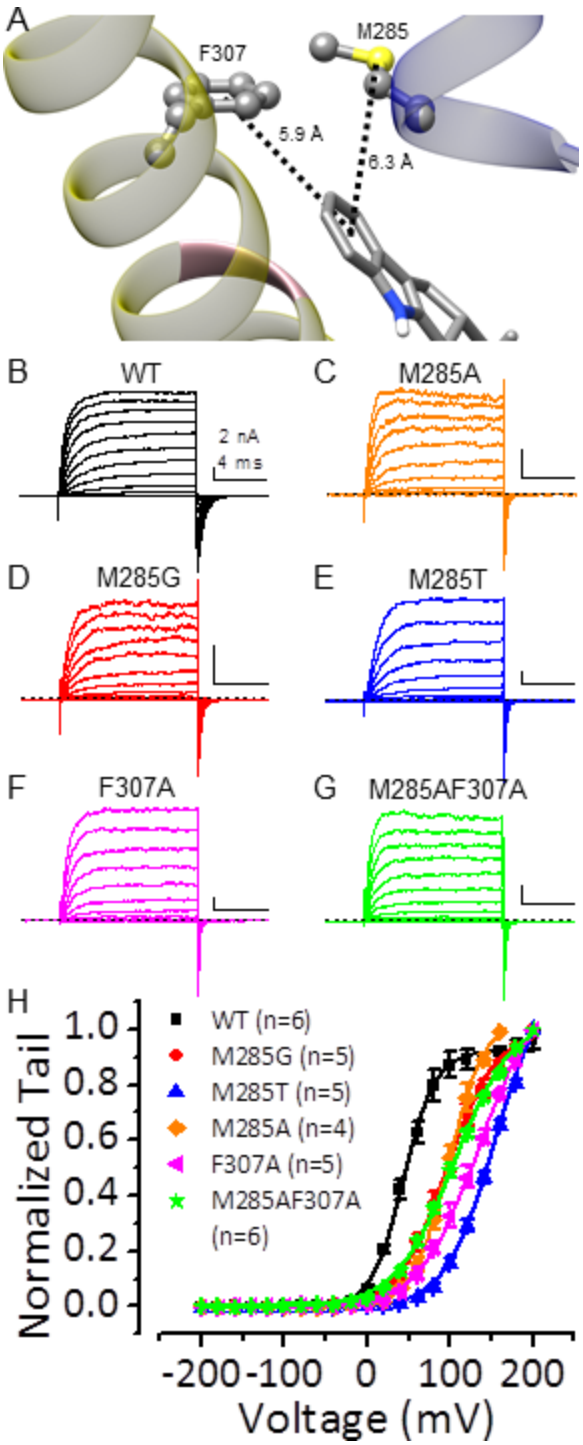

Fig. S10 Gating is positively shifted by mutations in the PAX binding crevice. (A) Potential PAX interacting residues in the binding crevice. F307 in the BK S6 and M285 in the BK pore-loop are rendered as ball-and-chain. PAX is rendered as stick. G311 is colored in pink. (B-G) Macroscopic currents of WT, M285A, M285G, M285T, F307A, and M285AF307A BK channels recorded from inside-out patches with 10 μM $[Ca^{2+}]_{in}$. The currents were evoked by steps from -200 to +200 mV with 20-mV increments. The dotted line marks the 0-current level. (H) The G-V

relationships of WT (black square), M285G (red circle), M285T (blue triangle), M285A (orange diamond), F307A (magenta triangle) and M285AF307A (green star) BK channels determined from the tail-current of recordings as those shown in panels B-G. The number of experiments contributing to each G-V relationship is listed in parentheses. Boltzmann fit results (solid lines) are: G_{max} = 0.9±0.01, V_h = 44.5±0.8 mV, z = 1.3±0.04e (WT), G_{max} = 1.0±0.01, V_h = 96.8±1.3 mV, z = 0.9±0.02e (M285G), G_{max} = 1.2±0.04, V_h = 154.7±2.7 mV, z = 0.8±0.04e (M285T), G_{max} = 1.0±0.02, V_h = 99.3±1.3 mV, z = 1.1±0.05e (M285A), G_{max} = 1.1±0.03, V_h = 133.4±2.3 mV, z = 0.7±0.03e (F307A), G_{max} = 1.0±0.02, V_h = 106.0±1.6 mV, z = 0.7±0.02e (M285AF307A).

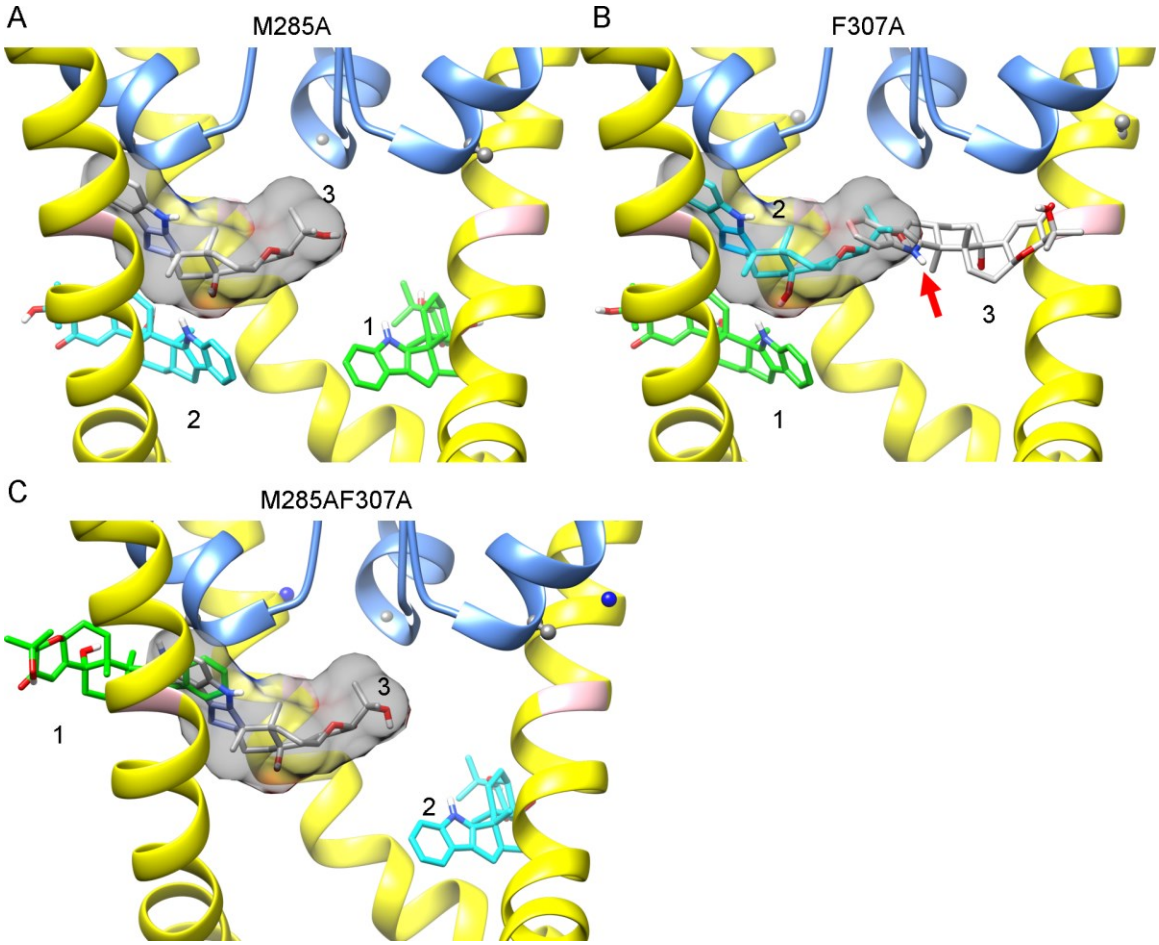

Fig. S11 Docking of PAX in the closed pore with binding crevice mutations. BK is rendered as ribbon with S6 and selectivity filter colored in yellow and blue, respectively. For clarity, the front subunit and all S5 segments are not shown. G311 is colored in pink to indicate the location of the PAX binding crevice. Mutated residues are rendered as ball-and-chain. PAX binding poses in mutated channels are rendered as sticks. (A) The top 3 unique binding poses of PAX in the closed mSlo1M285A structure. The numbers in this and following panels give the rank order of binding poses, with 1 being the best binding pose. The binding energies of poses No. 1 to 3 calculated by Autodock Vina are (in kcal/mol): -8.9, -8.8, -8.8. The binding pose No.3 is identical to the canonical binding pose in WT mSlo1 pore (semi-transparent surface in this and following panels), with rmsd of 0.325 Å between the two poses (B) The top 3 unique binding poses of PAX in the closed mSlo1F307A structure. The binding energies of poses No. 1 to 3 are (in kcal/mol): -8.8, -8.5, -8.3. The binding pose No.2 is identical to the canonical binding pose in WT mSlo1 pore, with rmsd of 0.124 Å between the two poses. It should be noted that even though binding pose No. 3 is also close to the binding crevice, the orientation of PAX is opposite to that observed in WT structure, with its indole ring (red arrow) pointing into the central cavity but not into the binding crevice. (C) The top 3 unique binding poses of PAX in the closed mSlo1M285AF307A structure. The binding energies of poses No. 1 to 3 calculated by Autodock Vina are (in kcal/mol):

-9.9, -9.0, -8.6. The binding pose No.3 is identical to the S6-Pore Helix crevice binding pose in WT mSlo1 pore, with rmsd of 0.284 Å between the two poses.

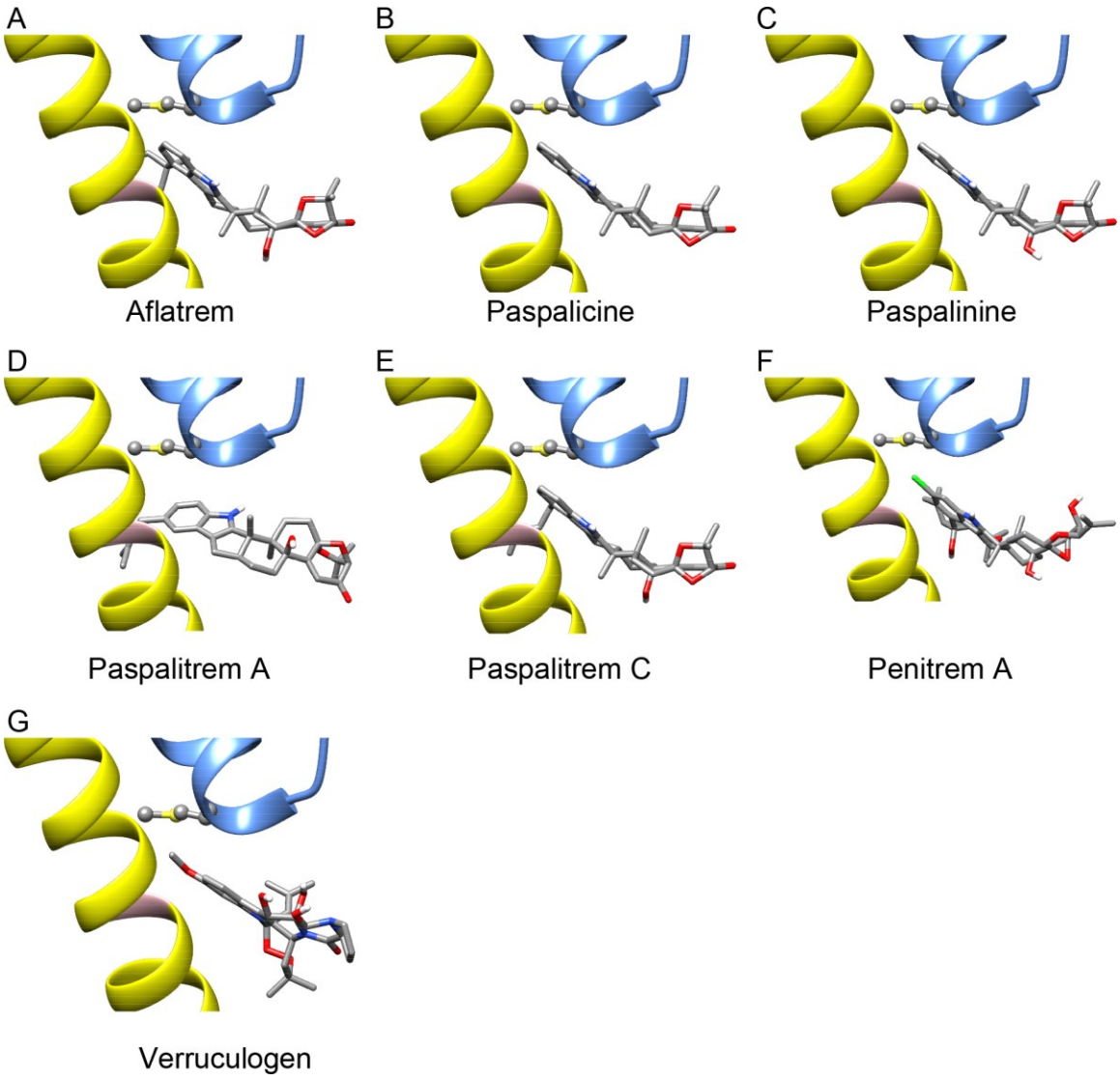

Fig. S12 The most favored binding poses of tremorgenic fungal alkaloids in closed mSlo1 pore. The perspective is the same as that of Fig. 2A. The S6 and selectivity filter of mSlo1 are colored in yellow and blue, respectively. G311 is colored in pink and M285 is rendered as ball-and-chain. (A) Aflatrem. (B) Paspalicine. (C) Paspalinine. (D) Paspalitrem A. (E) Paspalitrem C. (F) Penitrem A. (G) Verruculogen.

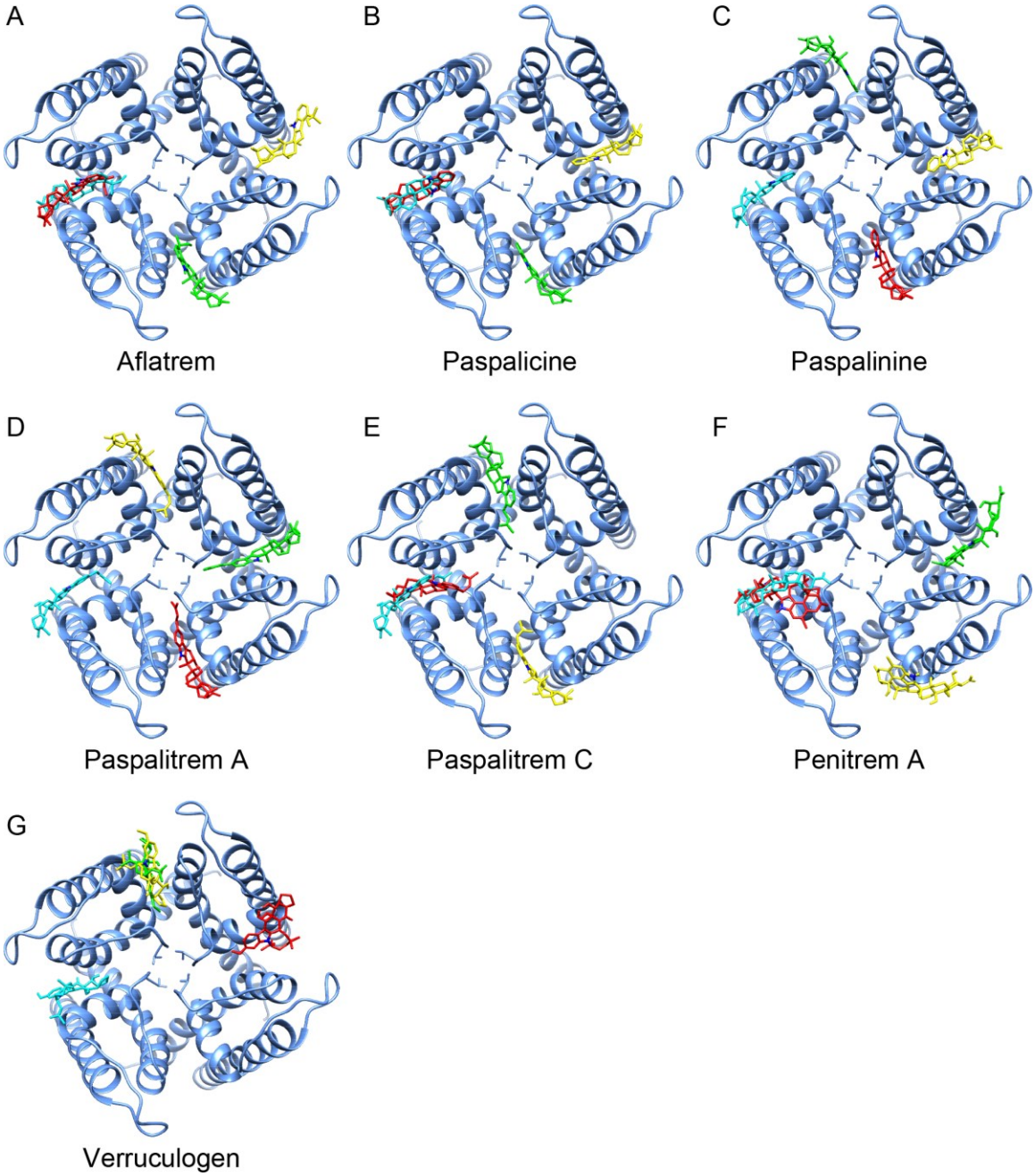

Fig. S13 The binding poses of tremorgenic fungal alkaloids in the open mSlo1 pore viewed from extracellular side. The top four unique binding poses are displayed for each compound, with No. 1-4 poses colored in cyan, green, yellow, and red, respectively. The nitrogen of indole ring is colored in blue to indicate the orientation of each binding pose. The binding energy of each binding pose is listed in Table S2.

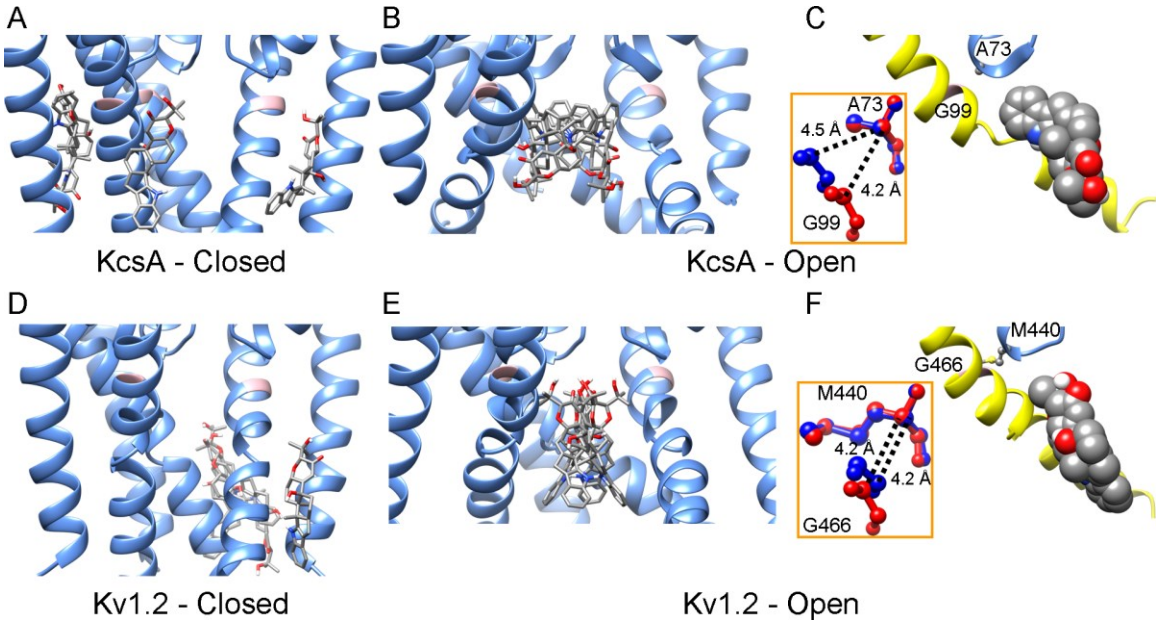

Fig. S14 The most favored docking poses of PAX in other K^+ channels. (A) Docking position of PAX in a closed KcsA channel structure (PDB: 1K4C). The glycine hinge (G99 of KcsA or G466 of Kv1.2) in this and all other structures shown in this figure is colored in pink. The front subunit is omitted for clarity. (B) Docking position of PAX in a wide-open KcsA channel structure (PDB: 3F5W). (C) A close-up view of the optimal PAX binding pose in the wide open KcsA pore. The perspective and coloring of this panel and panel F are identical to that of Fig. 2. The inset shows the dimension of the S6-PH crevice of closed (red) and open (blue) KcsA structures, as measured by the distance between the α-carbons of A71 and G99 (homologous to mSlo1 M285 and G311, respectively) in the same subunit. (D) Docking position of PAX in a closed Kv1.2 channel structure. (E) Docking position of PAX in an open Kv1.2 channel structure. (F) A close-up view of the optimal PAX binding pose in the open Kv1.2 pore. The inset shows the dimension of the S6-PH crevice of closed (red) and open (blue) Kv1.2 structures, as measured by the distance between the α-carbons of M440 and G466 (homologous to mSlo1 M285 and G311, respectively) in the same subunit.

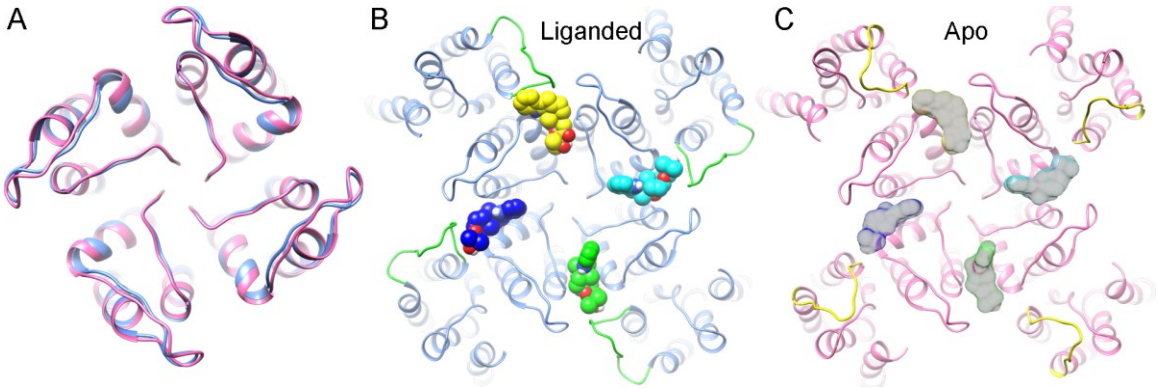

Fig. S15 The S1-S2 loop may contribute to extracellular binding of PAX. (A) Top view of the PGDs of open (blue) and closed (pink) mSlo1 models, with alignment based on their selectivity filters. (B) Top view of the 4 most favored unique PAX binding poses (spheres) in the open mSlo1 model. These poses are the same as that shown in SI Appendix Fig. S2B and colored in the same scheme, with the carbons of poses 1-4 colored blue, cyan, green and yellow, respectively. The S1-S2 linkers of the open mSlo1 model are colored in green. (C) Top view of the closed mSlo1 model (pink) with its S1-S2 linkers colored in yellow. The 4 most favored binding poses identified in the open model are included (semi-transparent surfaces) to show that the S1-S2 linkers in the closed model are tilted away from these poses.

SI REFERENCES

1. Zhou, Y, Xia, XM, Lingle, CJ, (2018) BK channel inhibition by strong extracellular acidification. Elife. **7**.

2. Tao, X, Hite, RK, MacKinnon, R, (2017) Cryo-EM structure of the open high-conductance Ca^{2+}-activated K^{+} channel. Nature **541**: 46-51.

3. Giangiacomo, KM, Becker, J, Garsky, C, Schmalhofer, W, Garcia, ML, Mullmann, TJ, (2008) Novel alpha-KTx sites in the BK channel and comparative sequence analysis reveal distinguishing features of the BK and KV channel outer pore. Cell Biochem. Biophys. **52**: 47-58.

4. Zhou, Y, Xia, XM, Lingle, CJ, (2011) Cysteine scanning and modification reveal major differences between BK channels and Kv channels in the inner pore region. Proc. Natl. Acad. Sci. U. S. A **108**: 12161-12166.

5. Chen, X , Aldrich, RW, (2011) Charge substitution for a deep-pore residue reveals structural dynamics during BK channel gating. J. Gen. Physiol **138**: 137-154.

6. Chen, X, Yan, J, Aldrich, RW, (2014) BK channel opening involves side-chain reorientation of multiple deep-pore residues. Proc. Natl. Acad. Sci. U. S. A **111**: E79-E88.